PLOS ONE

RESEARCH ARTICLE

Characterization of an undocumented CO_2 hydrothermal vent system in the Mediterranean Sea: Implications for ocean acidification forecasting

Michela D'Alessandro[1]*, **Maria Cristina Gambi**[1]*, **Matteo Bazzarro**[1], **Cinzia Caruso**[2], **Marcella Di Bella**[1,3], **Valentina Esposito**[1,4], **Alessandro Gattuso**[2], **Salvatore Giacobbe**[5], **Martina Kralj**[1], **Francesco Italiano**[2], **Gianluca Lazzaro**[2], **Giuseppe Sabatino**[1], **Lidia Urbini**[1], **Cinzia De Vittor**[1]

1 National Institute of Oceanography and Applied Geophysics – OGS, Trieste, Italy, 2 Istituto Nazionale di Geofisica e Vulcanologia – INGV, Palermo e Sede Operativa di Milazzo, Milazzo, Italy, 3 Sede Territoriale Sicilia, Department of Integrated Marine Ecology, Stazione Zoologica Anton Dohrn (SZN), Milazzo, Italy, 4 Stazione Zoologica Anton Dohrn, Research Infrastructures for Marine Biological Resources Department, Roma, Italy, 5 Department of Chemical, Biological, Pharmaceutical and Environmental Sciences, ChiBioFarAm, University of Messina, Messina, Italy

* mdalessandro@ogs (MD); mgambi@ogs.it (MCG)

Abstract

A previously undocumented shallow water hydrothermal field from Sicily (Southern Tyrrhenian Sea, Italy) is here described, based on a multidisciplinary investigation. The field, covering an area of nearly 8000 m^2 and a depth from the surface to -5 m, was explored in June 2021 to characterise the main physico-chemical features of the water column, describe the bottom topography and features, and identify the main megabenthic and nektonic species. Twenty sites were investigated to characterise the carbonate system. Values of pH ranged between 7.84 and 8.04, ΩCa between 3.68 and 5.24 and ΩAr from 2.41 to 3.44. Geochemical analyses of hydrothermal gases revealed a dominance of CO_2 (98.1%) together with small amounts of oxygen and reactive gases. Helium isotope ratios (R/Ra = 2.51) and $δ^{13}C_{CO2}$ suggest an inorganic origin of hydrothermal degassing of CO_2 and the ascent of heat and deep-seated magmatic fluids to the surface. Visual census of fishes and megabenthos (mainly sessile organisms) allowed the identification of 64 species, four of which are protected by the SPA/BIO Protocol and two by the International Union for Conservation of Nature. The macro-algae *Halopteris scoparia* and *Jania rubens* and the sponge *Sarcotragus* sp. were the dominant taxa in the area, while among fishes *Coris julis* and *Chromis chromis* were the most abundant species. This preliminary investigation of San Giorgio vent field suggests that the site could be of interest and suitable for future experimental studies of ocean acidification.

Introduction

Hydrothermal vents are worldwide recognized for their biological, ecological, cultural, and economic relevance [1, 2]. The upwelling of fluids makes them highly productive areas [3],

which provide notably ecosystem services such as provision, regulation and cultural services. Their relevant production is related to the high rates of chemosynthetic production by microbial communities that draw energy converting inorganic compounds such as H_2S, CH_4, and Fe^{2+} [4]. This high primary production leads to high biomass of invertebrates and fisheries resources, which in turn brings economic benefits to humans [3]. The benefits of hydrothermal vents also include the provision of metabolites and bioactive molecules produced by some organisms to survive in extreme conditions that are used by the cosmetic and pharmaceutical industries [5]. In addition, the uptake of sulphide and methane by bacteria reduces the emission of these substances into the atmosphere [6]. Additionally, recent findings have highlighted the role of vents in binding metals to organic molecules in seawater, creating organic-metallic complexes that increase their flux to the global ocean [2]. In terms of cultural services, hydrothermal ecosystems represent interesting study areas in various scientific fields, including studies on Ocean Acidification (OA) and the origin of life in the universe [7, 8]. In many vent systems, the bubbling of fluids makes the surrounding environment an ecological analogue of what is expected in future ocean scenarios as a consequence of OA [9–11]. For this reason, selected hydrothermal ecosystems are increasingly being used as natural laboratories to analyse species and community-level biological and physiological responses to OA [12, 13].

Hydrothermal fields are found at a wide depth range from the intertidal zone to the abyss and are characterized by different living communities [14, 15]. Generally, the deep hydrothermal vents (> 200 m) are inhabited by a typical fauna dominated by obligate taxa and symbiotic species which include siboglinid tubeworms, large bivalves, and snails [14]. Shallow-water (< 200 m) hydrothermal vent communities usually lack exclusive taxa and are often characterized by a simplification of the marine habitat resulting from a general reduction in species richness and abundance [15–17]. Despite their apparent similarity to near environments, shallow vents have provided new or rare species, although not as closely related to hydrothermal fluids as in oceanic deep-waters vents [18, 19].

The biological peculiarities distinguishing deep and shallow hydrothermal areas are mainly tied to differences in their chemical complexity. In fact, shallow hydrothermal systems are characterized by a lower pressure of fluids that can derive in different amounts from meteoric water, seawater, and magmatic fluid. Groundwater flow can be influenced by various sources, such as hydraulic gradient, rock type, anthropogenic pressure, and tidal pumping [20]. In contrast, deep-sea hydrothermal fluids are derived exclusively from seawater, except in special cases where magmatic fluids are involved [21, 22]. To date, about 25 shallow systems are known worldwide [23–25], but a significant number may not yet have been recognized [25].

In the Mediterranean, hydrothermal areas are reported from the Tyrrhenian, the Balearic and the Aegean Sea. Tyrrhenian hydrothermal fields are known in the Aeolian archipelago, i.e., at Vulcano, Stromboli, Filicudi and Panarea Islands and nearby islets, at Capo Palinuro, Ischia island and other sites within the Bay of Naples (Campania), at the Pontine Archipelago (Latium), [24–28], and Scoglio d'Africa (Tuscan Archipelago) [29]. In the Balearic Sea, a vent system has been described at the Columbretes islands [30], while in the Aegean Sea, major hydrothermal vent systems are found along the Volcanic Arc at Euboea, Milos, Santorini, Kos, and Yali Nisiros [24, 31]. In addition to the Mediterranean Sea, hydrothermal CO_2 emissions have been reported in shallow waters worldwide, both in oceans and lakes [32–34].

The recognition and characterization of hydrothermal vents are crucial for understanding the interactions between geochemical and biological processes on the seafloor. In particular, shallow hydrothermal vent ecosystems are of special interest due to their usually easy accessibility and suitability for experimental and manipulative research [14]. The aim of this paper is to provide the first multidisciplinary description of a previously undocumented CO_2-rich hydrothermal system in the southern Tyrrhenian Sea (northern coast of Sicily), in order to

characterize the area and discuss its suitability for experimental studies of ocean acidification.

Material and methods

Geological setting of the investigated hydrothermal area

The studied hydrothermal area is located at San Giorgio di Gioiosa Marea, Gulf of Patti NE Tyrrhenian coast of Sicily (S1 Table, Figs 1 and 2).

The area belongs to the regional tectonic structure known as the Aeolian-Tindari-Letojanni NW-SE faults system (ATLFS), which extends from the central sector of the Aeolian Islands (Salina, Lipari and Vulcano) to the Ionian Sea [35–38]. The ATLFS represents an incipient transfer zone separating a contractional domain to the west from an extensional one to the north-east (Fig 1). It represents one of the most seismically active regions of the Italian peninsula [37, 38] and is linked to the general geodynamic scenario of the central Mediterranean, characterised by the convergence between the European and African plates [39–41]. Recently, on the coast of the study area, CO_2 degassing was detected by Italiano et al. [28] along the southernmost section of the ATLFS (Nebrodi-Peloritani Mountains) suggesting a source in the crust and/or mantle for the fluid emissions in question. In addition, intense submarine volcanic processes and degassing activities have been reported in the nearby aeolian volcanic archipelago facing the study area, mainly on the islands of Vulcano and Panarea [42]. The CO_2 vents of Panarea represent the major hydrothermal systems of the entire Mediterranean Sea,
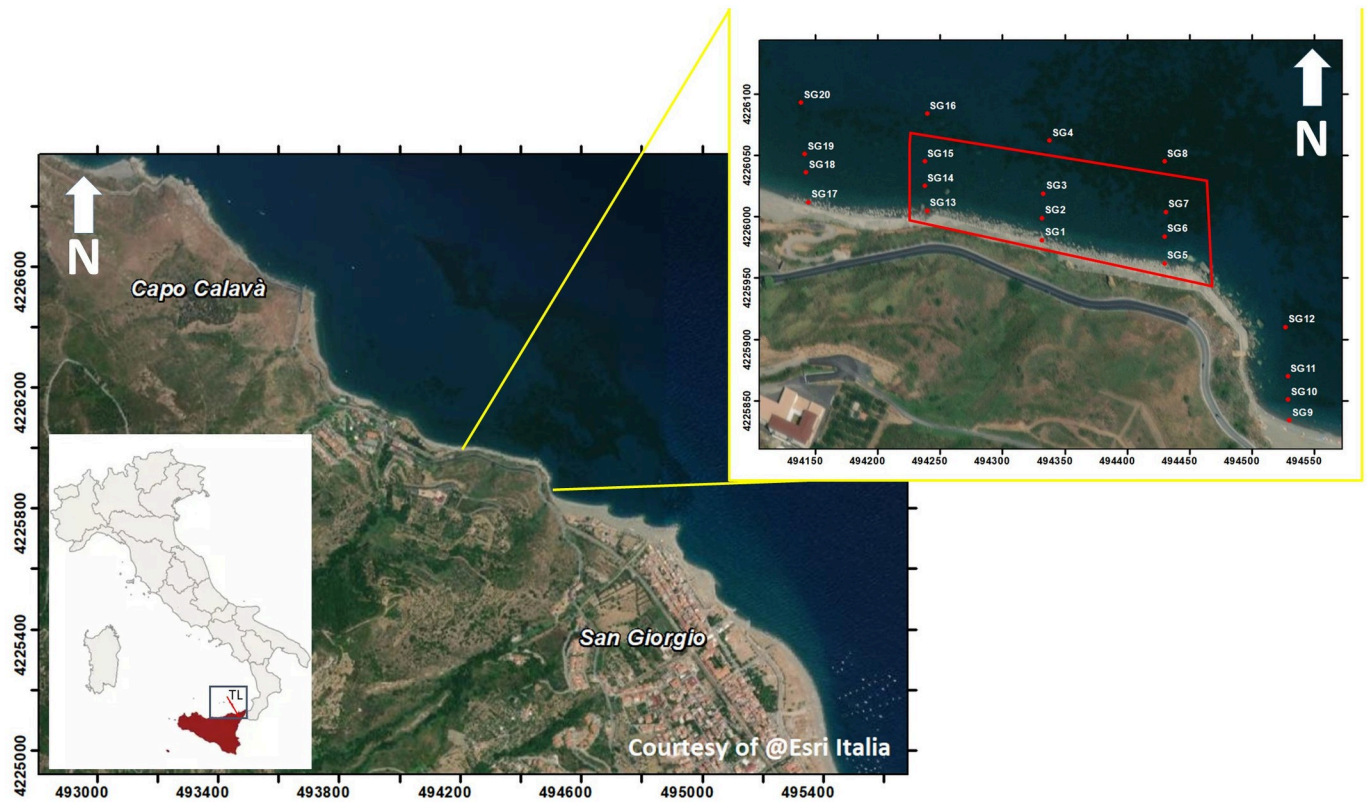

Fig 1. The study site. The hydrothermal field of San Giorgio is highlighted by the red polygon. TL: Aeolian-Tindari-Letojanni faults system. Map made by means of ArcMap 10.5, ESRI software.
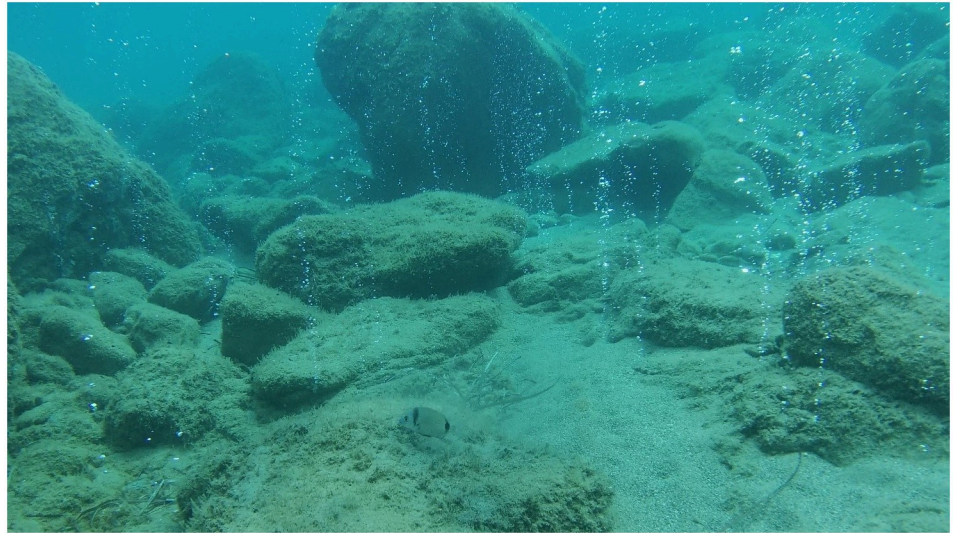
https://doi.org/10.1371/journal.pone.0292593.g001

Fig 2. One of the high intensity gas emissions from the San Giorgio hydrothermal vents.

https://doi.org/10.1371/journal.pone.0292593.g002

where a submarine gas eruption occurred in early November 2002 near the Bottaro rock, producing a submerged crater [43].

Sampling survey

A preliminary survey was conducted in May 2021 to obtain an initial overview of the pH variability of the area, define the spatial distribution of the system, develop a sampling plan, and select the most appropriate sampling and investigation techniques. In this first step, three water samples were collected on which only spectrophotometric pH analyses were performed according to the sampling procedure and laboratory methods explained below [43, 44]. In addition, a rectangular area approximately 200 m long and up to 40 m from the shoreline, covering the emission field, has been defined. Two different surveys were planned in this area, each aimed to characterise the main physico-chemical features and to conduct a visual census to verify the bottom topography and features, and to identify the main megabenthic and nektonic species.

Biological and chemical samplings were conducted in June 2021. Five transects perpendicular to the coastline were selected for seawater chemical analyses (Fig 1, S1 Table). A central transect (TR1) was established to intercept the point of highest emission flux at the seabed (SG2). Moving eastwards, the TR2 crosses the last emissions visible and the TR3 transect is located about 100 m far from TR2. The other two transects were established to the west of TR1 near the last visible emissions (TR4) and about 100 m away from it (TR5), respectively. In each transect, four sampling stations (SG) were established at 1, 20, 40, and 80 m from the shoreline reaching a maximum depth of 4 m, for a total of 20 stations, 9 of which within the hydrothermal field and 11 outside (transects TR3, TR5, and all sampling points 80 m from the shoreline). This sampling plan allowed us to assess the impact of emissions on the surrounding environment and the chemical differences among hydrothermal and not hydrothermal sites.

Biotic surveys were conducted using underwater visual census (UVC) in the area directly affected by the emissions (circumscribed by the red rectangle in Fig 1), using transects parallel to the shoreline to better assess local species diversity at similar depths. UVC observations were conducted in four transects along the shoreline length of the area (200 m) and spaced 10

m apart, covering an area of approximately 8000 m^2 and a depth range of 1 (TR A) to 4–5 m (TR D), (S2 Table).

Water chemistry analyses

Water samples for salinity, pH, total Alkalinity (A$_T$), dissolved inorganic nutrients, and H$_2$S determination were collected with Niskin bottles along the five transects perpendicular to the shoreline (TR1-TR5). For salinity determination, samples were collected in 200-mL glass bottles and stored at 4˚C in the dark. Salinity was measured at the Centre for Oceanographic Calibration and Metrology (CTMO) of OGS by means of a Guildline Autosal 8400B Laboratory Salinometer.

For pH and AT determinations, 120-mL borosilicate glass bottles were filled with seawater, poisoned with 100 µL of saturated mercuric chloride (HgCl$_2$) to halt biological activity, sealed with glass stoppers and stored in the dark at 4˚C until analysis. Analyses of pH and AT were performed using a Cary 100 Scan UV-visible spectrophotometer and a Mettler Toledo G20 with LAUDA L100, respectively, according to the laboratory procedures described by Dickson et al. [44] and Urbini et al. [45]. The analytical precision for pH was estimated to be ±0.002 pH$_T$ units. Accuracy and precision of the AT measurements on CRM were determined to be less than ±2.0 mmol kg^{-1}.

Samples for dissolved inorganic nutrients (nitrite, NO$_2$, nitrate, NO$_3$, ammonium, NH$_4$, phosphate PO$_4$, and silicic acid, H$_4$SiO$_4$) determination were filtered on 0.7 µm pore size glass-fibre filters (Whatman GF/F) and stored frozen (−20˚C) in polyethylene vials until laboratory analysis. Samples were defrosted and analysed colorimetrically using a segmented flow QUAATRO Seal Analytical AutoAnalyzer according to Hansen and Koroleff [46]. The detection limits for the method were 0.01 µM, 0.02 µM, 0.03 µM, 0.01 µM, and 0.01 µM for NO$_2$, NO$_3$, NH$_4$, PO$_4$, and H$_4$SiO$_4$, respectively.

Samples for hydrogen sulphide determination (H$_2$S) were collected in 40-mL vials adding 0.8 mL zinc acetate (ZnC$_4$H$_6$O$_4$), stored at 4˚C in the dark and then analysed spectrophotometrically using a VARIAN CARY 100 Scan spectrophotometer at 670 nm according to [47].

All the analyses were performed by the National Institute of Oceanography and Applied Geophysics (OGS) part at the laboratories in Trieste and part at the ECCSEL-ERIC NatLab Italy in Panarea.

Gas composition analyses

Gas analyses were performed to rule out the organic nature of the bubbling and to determine its hydrothermal features. Samples were collected from the submarine vents using an inverted funnel connected to two-way glass bottles [48]. The chemical composition of bubbling gases was determined by gas chromatography (GC) using an Agilent instrument with double TCD-FID detector and argon as carrier gas. Gas samples had been admitted to the GC by a syringe, and uncertainties are within ±5%. Measurements of the carbon isotopic composition ($\delta^{13}C_{CO2}$) of the derived gasses were performed using the Delta Plus XP IRMS equipped with a Thermo TRACE GC and an interface to the Thermo GC/C III. The results (expressed in $\delta^{13}C$ ‰) are for the V-PDB (Vienna-Pee Dee Belemnite) standard, and the standard deviation of the $^{13}C/^{12}C$ ratio was ±0.2‰. The He isotope ratio (^{3}He/^{4}He) was analysed using a Helix SFT-Thermo static vacuum mass spectrometer after purification of He under high vacuum and cryogenic separation of Ne. The isotopic composition of helium is reported as R/ RA, namely, ^{3}He/^{4}He of the sample versus the atmospheric ^{3}He/^{4}He (RA = 1:386 × 10–6). Typical uncertainties are within ±5%.

Fig 3. Measures of gas output flux from sediments by a INGV researcher at the San Giorgio vents.

https://doi.org/10.1371/journal.pone.0292593.g003

Five-point measurements of the gas flux were made to estimate the total gas output from the sediments, calculating the emptying time of a 1-litre bottle connected to the bubbling point via an inverted funnel (Fig 3).

These measurements were made in areas of low, medium, and high fluxes, as defined by visual evaluation of the bubbling emission intensity by divers.

In addition, measurements of gas ejection concentrations were made using an innovative, ad hoc instrument for determining air-water gas exchange rates. It consists of a floating platform equipped with a specially designed infrared spectrophotometer (IR) directly connected to the chamber. The main components are an infrared gas analyzer (IRGA—CO2 Infrared Gas Sensor Gascard NG 10%), a pump and an accumulation chamber (S1 Fig). The chemical and isotopic analysis was performed in the laboratories of INGV-Palermo.

Environmental description and biotic investigation

Data on benthic and nektonic organisms and associated bottom features were acquired through videos and photos from high-resolution cameras (Crosstour Action Cam 4K). Species directly identified in the field were recorded on a slate (S2 Table).

To calculate species and habitats frequency, videos of each transect parallel to the coast were analysed by selecting one frame every 10 seconds, corresponding to a linear distance of 2–3 m. In the selected plots (approx. 1x1 m frame), we estimated the percentage cover of different substrate types, such as soft sediments (sands), stones (smaller than 1 m), boulders (> 1 m) and rocks, and the seagrass *Posidonia oceanica*; we also annotated the occurring benthic organisms (plant and animals) and fishes in each plot. The frequency of these organisms on the transect was measured as the percentage of their occurrence over the total plots examined (S2 Table). The scientific name of each identified species was up-dated according to the WoRMS database ("https://www.marinespecies.org").

Statistical analyses

In order to evaluate potential differences in the composition of macrobenthic assemblages observed along the four transects explored during UVC and their spatial variability at different depths, each of the four 200 m video transects (TRA, TRB, TRC, and TRD) was divided into 8 segments of 25 m length each, resulting in 32 sampling units. This length unit was selected because it is considered the standard length for fish visual census in Mediterranean survey [49]. A one-way nonparametric multivariate analysis of variance (PERMANOVA) was then performed on the number of observations of each taxa recorded for each 25 m sampling unit.

The analysis was based on Bray-Curtis similarity analysis with 4999 random permutations calculated on square root transformed data. Terms that were found to be significant in the analysis (p<0.05) were examined individually using appropriate pairwise comparisons. Finally, a percent similarity (SIMPER) test and principal coordinate analysis (PCoA) were used to highlight the contribution of each taxon to the dissimilarities between transects.

All these analyses were performed using the statistical software applications PRIMER6 & PERMANOVA+ [50, 51].

Results

Water chemistry

The results of the chemical characterization of the water column are shown in S1 Table.

With the exception of stations SG1 and SG12 (37.77 and 37.82, respectively), the salinity along all transects shows the constant value of 37.79.

Regarding to carbonate system parameters (Fig 4), A_T ranged from 2521 µmol kg^{-1}, the minimum recorded at station SG3 (transect 1, depth 2.5 m), to 2533.5 µmol kg^{-1}, the maximum measured at station SG4 (transect 1, depth 5 m).

The pH values recorded during the pre-survey in May were generally lower than those measured in June: in SG2 pH_T May = 7.74, pH_T June = 7.84; in SG5, pH_T May = 7.82, pH_T June = 8.0; SG6, pH_T May = 7.83, pH_T June = 8.01. In June, the pH_T at *in situ* temperature showed generally lower values along transects 1 and 4, reaching the minimum of 7.84 at station SG2. The other transects appeared to be less affected by vents and had fairly homogeneous pH_T values, reaching the maximum (8.042) at station SG20. The lowest ΩCa out and ΩAr out were both recorded in SG2, with a value of 3.68 and 2.41, respectively.

All dissolved inorganic nutrients, generally had the highest concentrations in TR5, outside of the direct bubbling of the vents on the westwards side (Fig 5, S1 Table). Ammonia ranged from undetectable (<0.03 µmol L^{-1}, stations from SG10 to SG16) to 0.05 µmol L^{-1} (stations SG17 and SG18). Nitrite generally had concentrations of 0.01–0.02 µmol L^{-1} reaching the maximum of 0.04 in SG20. Nitrate showed very low concentrations along transects TR2, TR3 and TR4 (ranging from undetectable to 0.04 µmol L^{-1}), slightly elevated in TR1 (0.03–0.08 µmol L^{-1}) and increased in TR5, reaching a maximum of 0.56 µmol L^{-1} at SG20.
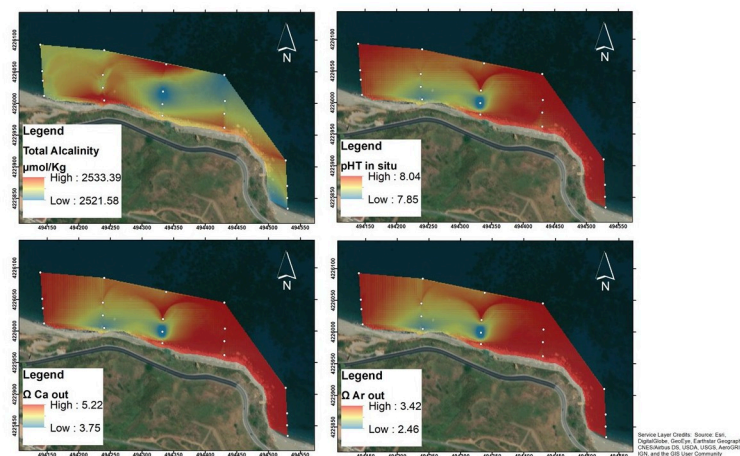

Fig 4. Natural neighbour spatial interpolations of total alkalinity, pH_T, Ω Ca and Ω Ar recorded in the San Giorgio vents study area. The map was created using ArcMap 10.5, ESRI software.
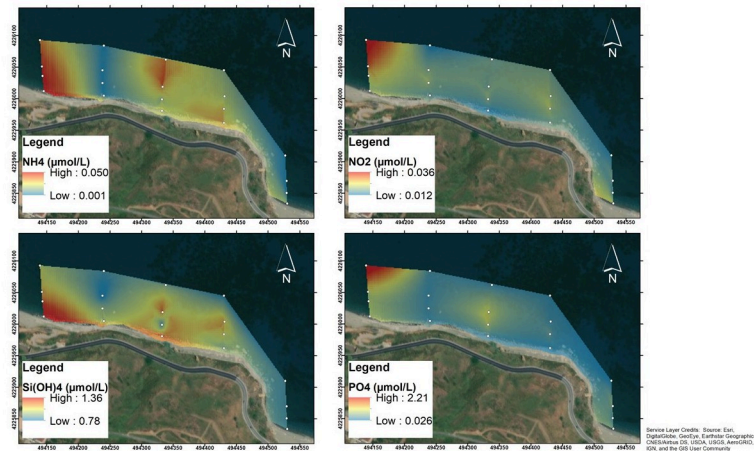
https://doi.org/10.1371/journal.pone.0292593.g004

Fig 5. Natural neighbour spatial interpolations of NH_4, NO_2, $Si(OH)_4$ and PO_4 recorded in the San Giorgio vents study area. The map was created using ArcMap 10.5, ESRI software.

https://doi.org/10.1371/journal.pone.0292593.g005

Silicates ranged from 0.78 µmol L^{-1} in SG15 (TR4) to 1.36 µmol L^{-1} in SG17 (TR5), with a mean value of 0.96 ± 0.15 µmol L^{-1}, while phosphates showed significant variations from 0.02 µmol L^{-1} (SG5, TR2) to 2.24 µmol L^{-1} (SG17, TR5).

Spectrophotometric analysis of H_2S showed the presence of this analyte, in low concentration (0.17 µM), only at station SG2, while it was undetectable at all other stations.

Gas composition

Gas analysis revealed CO_2 as the dominant gas component (98.1%), followed by N_2 (1.02%), CH_4 (0.43%), H_2S (0.35%) and O_2 (0.14%). In addition, very low percentages were found for He, H_2 and CO (0.0015, 0.0007, and 0.0005%, respectively). The isotopic ratios of helium display values in the range of 2.51 Ra (Table 1).

The most abundant percentage of CO_2 recorded at the air-water interface was of 1.73% (Table 2).

A total flux of gasses of 30.75 litres/minutes has been estimated to be emitted in the whole area of the San Giorgio hydrothermal vents (Table 3).

Environmental description and biotic investigation

The seafloor, as observed along all transects parallel to the shoreline, consists of a mosaic of coarse sediments (mainly coarse sands) interspersed with stones (< 1 m), rocks/boulders (> 1 m), and patches of *Posidonia oceanica*. Sub-circular rusty patches occur on the sandy soil where intense venting occurs, ascribable to precipitation of metal oxides. The hard bottom areas (rocks or large boulders) close to the emissions are frequently colonized by microbial white mats. A total of 62 taxa were identified: 9 macrophytes, 29 invertebrates, and 24 fish (see list in S2 Table).

Table 1. Chemical and isotopic compositions of the sampled gas emissions. All the chemical concentrations are expressed in mol%. The helium isotopic composition is expressed as R/Ra, where R is the 3He/4He ratio in the sample and Ra is the same ratio in the atmosphere. The carbon isotopic composition is given versus PDB.

R/Ra	He/Ne	$\delta^{13}C_{CO_2}$	He %	H_2%	O_2%	N_2%	CO %	CH_4%	CO_2%	H_2S %
2.51	177.22	3	0.0015	0.000698	0.14	1.02	0.0005	0.43	98.1	0.35

https://doi.org/10.1371/journal.pone.0292593.t001

Table 2. Percentage of CO_2 recorded on four samples of air-water layer collected on the SG2 station. Coordinates are expressed in UTM WGS84, Zone 33 S.

	North (m)	East (m)	CO_2%
# 1	4226017	494330	0.7
# 2	4226016	494331	1.17
# 3	4226019	494332	0.85
# 4	4226024	494335	0.35

https://doi.org/10.1371/journal.pone.0292593.t002

Among the algae, all species found were typical of the shallow photophilous hard bottoms, including *Padina pavonica*, *Halopteris scoparia*, *Anadyomene stellata*, *Corallina elongata*, *Jania rubens* and *Codium bursa*. Among the invertebrates, the sponge *Sarcotragus* sp. is the most common sessile organism, while most of the other invertebrate species were molluscs (25%), mainly gastropods associated with vegetated hard bottoms, but the bivalves *Chamelea gallina* and *Donax trunculus* were also found associated with sandy substrates. Moreover, the bivalve *Pinna rudis* was recorded, associated with *Posidonia* meadows. In fact, an extensive meadow of the seagrass *Posidonia oceanica* extends at the edge of the vent's field. Three non-indigenous species were recorded, the green alga *Caulerpa cylindracea*, *Caulerpa taxifolia var. distichophylla* and the crab *Percnon gibbesi*. The 24 species characterizing the ichthyofauna include *Coris julis*, *Chromis chromis*, *Diplodus annularis*, *Mullus barbatus*, *Thalassoma pavo*, *Trachinotus ovatus* and juveniles of two *Epinephelus* species, namely *E. costae* and *E. marginatus*, both considered as vulnerable and endangered in the IUNC list. Juveniles of several other bony fishes were recorded, such as *C. chromis*, *Diplodus vulgaris*, *M. barbatus*, *T. ovatus*, *T. pavo*, *Symphodus tinca* and *Sparisoma cretense*.

A brief description of each transect is provided below to characterize the main bottom features and the most frequent benthic and fish species.

Transect A (approx. 1 m depth, 109 plots analysed): the bottom is dominated by stones and sand, overall counting about the same frequency percentage of plots (82.6 and 81.7%, respectively). Boulders/rock were recorded in 22% of the plots. Very few tufts of *P. oceanica* were observed (2.7% of plots). Both boulders/rock and stone were characterized by a prevalent algal cover (92.7% of plots) mainly represented by turf and erected algae, with sparse sponges. The species recorded with the highest frequency was *Halopteris scoparia* (47.7% of the plots), followed by *Jania rubens* (28.4%), and by the sponge *Sarcotragus* sp. (14.7%). Several species were recorded with frequencies less than 10%, as the coralline alga *Corallina elongata* (7.3%), the sponges *Ircinia irregularis* (5.5%) and *Crambe crambe*, the green alga *Anadyomene stellata*, and the cnidarian *Pennaria disticha* (both with 2.8%). The gastropods *Patella caerulea* (1.8%), *Stramonita haemastoma* (0.9%) and *Cerithium vulgatum* (0.9%) were also observed on the rocks and stones.

Table 3. Total output of gasses and typologies of emission flux recorded on five different sites.

	Output (litres/min)	Point emissions	Measured emissions	Total output (litres/ min)	Typology of emissions
Flux 1	1	14	1	14	High
Flux 2	1.2	5	1	6	High
Flux 3	0.25	15	1	3.75	Medium
Flux 4	0.1	40	1	4	Low
Flux 5	0.1	30	1	3	Low

https://doi.org/10.1371/journal.pone.0292593.t003

Gas emissions of different intensities occurred in 5 scattered and 7 continuous plots. Along the transect, 12 bony fish species were observed, with *S. tinca* (17.4%) being the most frequent, followed by *C. chromis* (12%), and *D. vulgaris* (10%). The lowest frequencies were recorded for *E. costae* and *E. marginatus* (both with 0.9%).

In transect B (approx. 2 m depth, 96 plots analysed), the seafloor is composed of a mosaic of different substrate types: stones, occurring in 92.6% of the plots and covering a mean of 54% of the seafloor, followed by boulders/rock with 57% frequency and 50% covering, sands, although present in 82% of the examined plots, covered only a mean of 10% of the sea bottom. Stones showed a mean colonization by benthic organisms of 55%, while boulders/rock showed a mean colonization of 65%. *Posidonia oceanica* was present with very small patches in 22% of the plots and with a modest mean cover of 12%. Finally, gas emissions of different intensity were detected in 13 scattered and 4 contiguous plots. Stones and rocks were mainly colonized by a turf of small filamentous algae (97% of plots), followed by 4 macroalgae species such as *Padina pavonica* (78.1%), *J. rubens* (58.3%), *H. scoparia* (32.6%) and *A. stellata* (7.3%). Among invertebrates, only the sponge *Sarcotragus* sp. was dominant, occurring in 73% of the plots. Some gastropods were recorded with modest frequency, i.e., the sessile *Vermetus triquetrus* (3%), and the motile *Hexaplex trunculus* (4%). Seven taxa of bony fishes were observed, all with low frequencies: *C. chromis* (6.3%), *S. salpa* (4.2%), *D. vulgaris* (3.1%), *O. melanura*, *S. cabrilla*, *T. pavo*, *Tripterygion* sp. (all with 2.1%).

On transect C (approx. 2.5–3 m depth; 85 plots examined) the seafloor still shows a mosaic of different substrates, but an increase in boulders/stones (64% of the plots) with higher mean bottom cover (59%), and a higher frequency of Posidonia patches was also observed, occurring in 62% of the plots and with a mean cover of 23.4%. Sand patches are still frequent (63%) although with modest mean cover (17%). Gas emissions were encountered in 3 scattered and 4 contiguous plots. At this depth, both stones and rocks show much higher levels of benthic colonization compared to transect B, with a mean of 66.8% for stones and 85% for boulders/rocks. The hard substrates continued to be colonized mainly by turf algae (95.5%) and by the four previously mentioned macroalgae, which increased their frequencies: *J. rubens* (72.9%), *P. pavonica* (89.4%), *H. scoparia* (71%), *A. stellata* (7.1%). Among invertebrates, the most conspicuous species was still *Sarcotragus* sp. (77.7%), followed by *V. triquetrus* (6%), the sponge *Crambe crambe* (3.4%), and colonial hydroids (likely *Eudendrium* sp.) (2.3%). Along the transect, 7 fish species were observed: *S. salpa* (5.9%), followed by *D. vulgaris* (4.7%) and *O. melanura* (3.5%). Lower frequencies were recorded for *C. chromis*, *C. julis* (both 2.4%), *T. pavo* and *M. barbatus* (both 1.2%).

On transect D (approx. 4–4.5 m depth; 89 plots examined), the bottom is mainly characterized by sand (83.1%) mostly covered by *P. oceanica* (77.5%). Lower frequencies were recorded for stones (43.8%) and boulders/rock (7.9%), which showed high mean coverage percentages, 88.3% for boulders/rocks and 92.5% for stones. Only low intensity gas emissions were observed in 2 scattered and 4 continuous plots. The species showing the high frequencies were *P. pavonica* (33.7%), *J. rubens* (13.5%) *Sarcotragus* sp. (7.9%). Lower frequencies were recorder for the sponge *C. crambe* (1.1%) and the alga *A. stellata* (3.4%). Six fish species were encountered: *C. chromis* (21.3%), *S. maena* (7.9%), *O. melanura* (5.6%), *C. julis* and *D. vulgaris* (both with 2.2%), and *T. pavo* (1.1%).

Statistical results

The results of the statistical analysis on the 25 m units of each transect, evidenced significant differences among the macrobenthic assemblages of the four transects (PERMANOVA $F_{3,31} = 13.092$; $p<0.01$). Pairwise comparisons showed significant differences between all
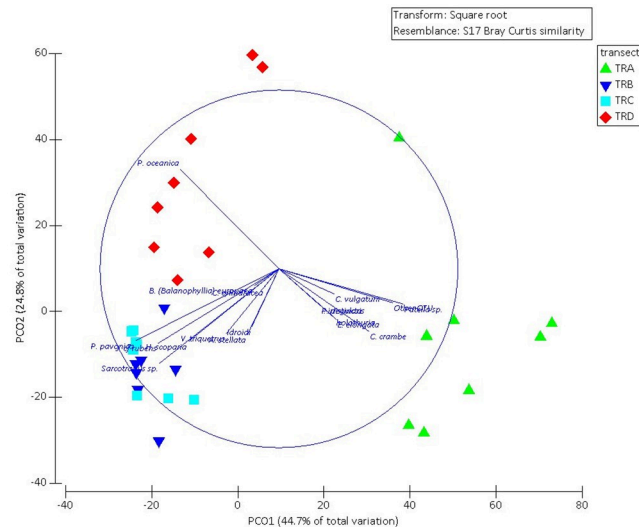
Fig 6. Principal coordinates analysis (PCoA) based on the number of observations of each macrobenthic taxon along the UVC transects. The overlaid vectors report the taxon that mostly contributed to the differences among transects.

pairs of factor levels considered (p<0.01), except between the two central transects (TRB and TRC). This pattern is also evident in the distribution of the points in the PCoA diagram (Fig 6), whose first two ordination axes explain 69.5% of the total variance. The overlaid vectors in the PCoA biplot and the results of the SIMPER test showed the highest average dissimilarity between the shallowest (TRA) and deepest (TRD) transects, mainly due to the bivalve *Patella* sp., which was observed most frequently along TRA, and the seagrass *P. oceanica*, which was observed mainly along TRD. The other two transects (TRB and TRC) shared four of the most frequently observed species: the sponge *Sarcotragus* sp. and the algae *P. pavonica*, *J.* cfr *rubens* and *H. scoparia*.

Discussions and conclusions

Shallow, CO_2-rich hydrothermal vents provide unique opportunities to study the vulnerability of coastal ecosystems to ocean acidification [52]. In this context, the undocumented San Giorgio vent (southern Tyrrhenian Sea), due to its physico-chemical features and easy accessibility, is an appropriate case of study, suitable as a natural laboratory to study ocean acidification and related changes in benthic and fish population structure and habitat complexity [53]. Even if, no other bubbling gasses and fluids were observed in the neighbouring areas during the study, the presence of other emissions cannot be ruled out given the geological setting of the study area, which is located along the Aeolian-Tindari-Letojanni faults system [36–38]. In this area, the pH value of 7.84 at the point of maximum emission flux, in the centre of the field indicates an intermediate level of acidification corresponding to the most reliable prediction for the year 2100 [54]. This value is comparable to those reported for the intermediate bubbling areas of the Castello Aragonese vents on Ischia (S2 and N2 stations of various publications) [14], whose pH, however, showed a great variability [55, 56] and a clear gradient, ranging from < 6.0 to 8.1, due to the high intensity of vents in the most acidified zone, to normal pH conditions outside the vent area. At San Giorgio, the pH range is also similar to that reported for the lower pH zone in Baia di Levante at Vulcano (7.84 ± 0.24 pH) [57], as well as with the

rim zone around Bottaro crater off Panarea island [58], in contrast with the very low values measured off Panarea around Basiluzzo island (pH 4.7–5.4) [59]. The contribution of the vents to the dissolved inorganic nutrient budget is apparently negligible, as suggested by the relatively low concentrations that increase in the outer part of the vent area, probably due to anthropogenic and terrigenous inputs.

The gasses emitted at the hydrothermal vents of San Giorgio have a predominant CO_2 composition similar to those measured in Levante Bay (Vulcano Island) (97–99%) [57] and slightly higher than those measured in Castello Aragonese (90–95%) [14, 40]. The percentage of H_2S (0.35%) in San Giorgio is lower than at Vulcano (2.2%) [60], while no sulphur occurs at the Castello Aragonese [40]. This very low percentage of H_2S, notably a toxic gas, favours investigations on the response of species and communities to ocean acidification. Indeed, in some vents the co-presence of CO_2 with other toxic gasses or high metal ion concentration, makes it difficult to separate the negative effects of OA from those of other hazardous substances [61, 62]. The high R/Ra values measured in the San Giorgio vents could be related to the ascent of heat and deep magmatic fluids to the surface. These values are similar to those measured at Capo Calavà (R/Ra = 2.5) in a gas sample collected about 2 km WNW of the investigated area by Sano et al. [63]. The value of $\delta^{13}C_{CO_2}$ seems to confirm an inorganic origin of the hydrothermal degassing of CO_2 [63]. Although no significant temperature differences were observed along the entire investigated area in our study, the observed sub-circular rusty patches, detected around the intense bubbling, could indicate an upwelling of mineral-enriched fluid columns into the seafloor, which needs to be further investigated.

Most of the species recorded in the San Giorgio vents are typical of shallow photophylous vegetated habitat and are commonly recorded in similar areas not subjected to gas emissions. The main algae dominating the rock and boulder coverage develop typically in summer (e.g., *P. pavonica*, *H. scoparia*), so that further important information could be acquired by sampling at the vents in different seasons. However, the dominat taxon along all transects and depths examined, is the perennial sponge *Sarcotragus* sp. Sponges are quite robust to OA, in accordance with their occurrence at other vent's systems as at Castello Aragonese [64], Grotta del Mago cave [40], and Vullatura vents at Ischia; although in this latter system the community is dominated by *C. crambe* settled on dead matte of *Posidonia oceanica* [40]. Moreover, four species listed in Annexes I and II of the SPA/BIO Protocol of the Barcelona Convention were detected: the scleractinian *Cladocora caespitosa*, the sea urchin *Paracentrotus lividus*, the relatively rare bivalve *Pinna rudis* and the seagrass *Posidonia oceanica*. The macrobenthic community shows a homogeneous pattern along the transects, but exhibits differences between transects, especially between the shallowest and deepest transects, which also show the highest spatial variability. The shallowest transect is characterized by an impoverished habitat dominated by boulders and poorly colonised, while the deepest transect is characterized by a Posidonia meadows which show a quite patchy distribution. The central transects, characterized by more intense bubbling and lower pH values, showed a more homogeneous and similar macrobenthic community, characterized by species relatively tolerant to ocean acidification, such as *Sarcotragus* sp. and *C. crambe*, as also observed in other vent systems [64]. The fish fauna resembles that found in other analogous areas of the Mediterranean Sea, as reported for the vents at Castello on Ischia and in Levante Bay on Vulcano [64, 65]. Similarly, to other shallow hydrothermal fields, no obligate taxa were identified in San Giorgio, whose communities were characterized by species, such as *S. salpa*, *C. chromis*, *C. julis*, known for their tolerance to acidification [64]. Although experimental studies have shown some negative effects of acidification on fish physiology and behaviour, especially on juvenile stages [65, 66], the San Giorgio vent field would seem a nursery area, with occurrence of many juveniles of several species. In addition, juveniles of *Epinephelus costae* and *E. marginatus*, considered respectively as

vulnerable and endangered species in the red list of threatened species enacted by the International Union for Conservation of Nature (IUCN), were also recorded.

Finally, differently than in other vents where alien organisms are often quite abundant, being favoured by low competition [27], a very low presence of alien species has been recorded in San Giorgio vent area, since limited to low covering by the alga *C. cylindracea* and sporadic occurrence of the decapod *P. gibbesi*.

In conclusion, although further investigation is necessary, the hydrothermal vent system of San Giorgio in Gioiosa Marea characterized by predominant CO_2 emissions and negligible presence of other potentially toxic compounds such as H_2S, could be elected as a suitable natural laboratory to study the effects of OA on marine ecosystem processes, also benefiting from its easy accessibility and shallow depth.

Even if, hydrothermal vents are recognized as biodiversity hotspots and provide important ecosystem services, no protection measures have been proposed in the Mediterranean Sea. In the Natura 2000 network [67], habitat No. 1180, "Submarine structures made by leaking gases", is considered as a habitat to be protected, but this definition is vague and seems to refer more to the geological nature rather than to the related biological aspects. We believe that the rarity of shallow hydrothermal vents and their ecological and evolutionary relevance require a better definition and explanation of 1180 habitat, bringing to include the biotic components associated with hydrothermal vents and their wide variability at local scales in order to apply conservation measures and give more attention to these unique ecosystems.

Supporting information

S1 Table. Values of the physico-chemical variables measured in transects sampled perpendicular to the coastline off the San Giorgio vent area. TR1 = central transect intercept the points of highest bottom flow of emissions. TR2 = transect moving eastward in correspondence with the last emissions visible. TR3, about 100 m far from TR2. TR4 = transect moving westward in correspondence with the last emissions visible. TR5 = about 100 m far from TR4. In each transect four sampling stations (SG) were located at 1, 20, 40 and 80 m away from the shoreline, reaching 4.5 m of maximum depth.
(DOCX)

S2 Table. List of species visually recorded in the San Giorgio hydrothermal vent studied. Species without values of frequency for all transects are those recorded only during the explorative survey.
(DOCX)

S1 Fig. Gas output instrument. Fig 1. Draft of the Gas Output Instrument to measure the air-water gas exchange. Fig 2. INGV researcher positioning the Gas output instrument on a sampling site off the San Giorgio vents.
(DOCX)

Acknowledgments

Author Contributions

Conceptualization: Michela D'Alessandro, Maria Cristina Gambi, Marcella Di Bella, Valentina Esposito, Salvatore Giacobbe, Francesco Italiano, Lidia Urbini, Cinzia De Vittor.

Data curation: Maria Cristina Gambi.

Formal analysis: Michela D'Alessandro, Maria Cristina Gambi, Matteo Bazzarro, Valentina Esposito, Martina Kralj, Lidia Urbini, Cinzia De Vittor.

Investigation: Michela D'Alessandro, Cinzia Caruso, Valentina Esposito, Alessandro Gattuso, Francesco Italiano, Gianluca Lazzaro, Giuseppe Sabatino.

Methodology: Michela D'Alessandro.

Resources: Cinzia De Vittor.

Supervision: Maria Cristina Gambi, Cinzia De Vittor.

Writing – original draft: Michela D'Alessandro, Maria Cristina Gambi, Matteo Bazzarro, Cinzia Caruso, Marcella Di Bella, Valentina Esposito, Alessandro Gattuso, Salvatore Giacobbe, Martina Kralj, Cinzia De Vittor.

Writing – review & editing: Michela D'Alessandro, Maria Cristina Gambi, Salvatore Giacobbe, Cinzia De Vittor.

References

1. Yang K, Scott SD. Possible contribution of a metal-rich magmatic fluid to a sea-floor hydrothermal system. Nature 1996; 383(6599): 420–423.

2. Sander SG, Koschinsky A. Metal flux from hydrothermal vents increased by organic complexation. Nat Geo. 2011; 4(3): 145–150.

3. Levin LA, Baco AR, Bowden DA, Colaco A, Cordes EE, Cunha MR et al. Hydrothermal vents and methane seeps: rethinking the sphere of influence. Front Mar Sci. 2016; 3: 72.

4. McCollom TM, Shock EL, Geochemical constraints on chemo-lithoautotrophic metabolism by microorganisms in seafloor hydrothermal systems. Geochim Cosmochim. 1997; Acta 61(20): 4375–4391.

5. Gurunathan R, Rathinam AJ, Hwang JS, Dahms HU. Shallow Hydrothermal Vent Bacteria and Their Secondary Metabolites with a Particular Focus on Bacillus. Mar Drugs. 2021; 19(12): 681. https://doi.org/10.3390/md19120681 PMID: 34940680

6. Boetius A, Wenzhöfer F. Seafloor oxygen consumption fuelled by methane from cold seeps. Nat Geosci. 2013; 6(9): 725–734.

7. Di Bella M, Pirajno F, Sabatino G, Quartieri S, Barbieri R, Cavalazzi et al. Rolling Ironstones from Earth and Mars: Terrestrial Hydrothermal Ooids as a Potential Analogue of Martian Spherules. Minerals. 2021; 1(5): 460.

8. Martin W, Baross J, Kelley D, Russell MJ. Hydrothermal vents and the origin of life. Nat Rev Microbiol. 2008; 6(11): 805–814. https://doi.org/10.1038/nrmicro1991 PMID: 18820700

9. Foo SA, Byrne M, Ricevuto E, Gambi MC. The carbon dioxide vents of Ischia, Italy, a natural laboratory to assess impacts of ocean acidification on marine ecosystems: an overview of research and comparisons with other vent systems. Oceanogr Mar Biol Ann Rev. 2018; 56: 237–310.

10. Dahms HU, Schizas NV, James RA, Wang L, Hwang JS. Marine hydrothermal vents as templates for global change scenarios. Hydrobiologia. 2018; 818 (1): 1–10.

11. Gonzalez Delgado S, Hernadez JC. The importance of natural acidified systems in the study of ocean acidification: what have we learned? Adv Mar Biol. 2018; 80: 57–99. https://doi.org/10.1016/bs.amb.2018.08.001 PMID: 30368306

12. González-Delgado S, González-Santana D, Santana-Casiano M, González-Dávila M, Hernández CA, Sangil C, et al. Chemical characterization of the Punta de Fuencaliente CO_2-enriched system (La Palma, NE Atlantic Ocean): a new natural laboratory for ocean acidification studies. Biogeosciences. 2021; 18(5): 1673–1687.

13. Harvey BP, Kon K, Agostini S, Wada S, Hall-Spencer JM. Ocean acidification locks algal communities in a species-poor early successional stage. Glob Change Biol. 2021; 27(10): 2174–2187.

14. Tarasov VG, Gebruk AV, Mironov AN, Moskalev LI. Deep-sea and shallow-water hydrothermal vent communities: two different phenomena? Chem Geol. 2005; 224 (1–3): 5–39.

15. Tarasov VG. Effects of shallow-water hydrothermal venting on biological communities of coastal marine ecosystems of the Western Pacific. Adv Mar Biol. 2006; 50: 267–421. https://doi.org/10.1016/S0065-2881(05)50004-X PMID: 16782453

16. Hall-Spencer JM Belfiore G Tomatsuri M Porzio L Harvey BP Agostini S. Decreased diversity and abundance of marine invertebrates at CO2 seeps in warm-temperate Japan. Zool Sci; 2022; 39 (1): 41–51. https://doi.org/10.2108/zs210061 PMID: 35106992

17. Agostini S, Harvey BP, Milazzo M, Wada S, Kon K, Floc'h N et al. Simplification, not "tropicalization", of temperate marine ecosystems under ocean warming and acidification. Glob Chang Biol 2021; 27 (19): 4771–4784. https://doi.org/10.1111/gcb.15749 PMID: 34268836

18. Giangrande A, Gambi MC, Micheli F, Kroeker KJ. Fabriciidae (Annelida, Sabellida) from a naturally acidified coastal system (Italy) with description of two new species. J Mar Biolog Assoc. 2014; 94(7): 1417–1427.

19. Giangrande A, Putignano M, Licciano M, Gambi MC. The Pandora's box: Morphological diversity within the genus emAmphiglena/em Claparède, 1864 (Sabellidae, Annelida) in the Mediterranean Sea, with description of nine new species. Zootaxa. 2021; 4949 (2).

20. Teixidó N, Gambi MC, Parravacini V, Kroeker K, Micheli F, Villéger S, et al. Functional biodiversity loss along natural CO_2 gradients. Nat Comm. 2018; 9(1): 1–9.

21. Gamo T, Glasby GP. Submarine hydrothermal activity in coastal zones. In Land and Marine Hydrogeology. Elsevier: 2003; pp. 151–163.

22. Gamo T, Okamura K, Charlou JL, Urabe T, Auzende JM, Ishibashi J, et al. Acidic and sulfate-rich hydrothermal fluids from the Manus back-arc basin, Papua New Guinea. Geology. 1997; 25(2): 139–142.

23. Martorelli E, Italiano F, Ingrassia M, Macelloni L, Bosman A, Conte AM, et al. Evidence of a shallow water submarine hydrothermal field off Zannone Island from morphological and geochemical characterization: Implications for Tyrrhenian Sea Quaternary volcanism. J. Geophys. Res. Solid Earth. 2016; 121 (12): 8396–8414.

24. Daskalopoulou K, D'Alessandro W, Longo M, Pecoraino G, Calabrese S. Shallow Sea Gas Manifestations in the Aegean Sea (Greece) as Natural Analog to Study Ocean Acidification: First Catalog and Geochemical Characterization. Front Mar Sci. 2022; 8: 775247.

25. Dando PR, Stüben D, Varnavas SP. Hydrothermalism in the Mediterranean Sea. Prog Oceanogr. 1999; 44(1–3): 333–367.

26. Preston V., Flaspohler G., Kapit J., Pardis W., Youngs S., Martocello III, et al. Discovering hydrothermalism from Afar: In Situ methane instrumentation and change-point detection for decision-making. Front Earth Sci. 2022; 10:984355.

27. Hall-Spencer JM, Allen R. The impact of CO_2 emissions on "nuisance" marine species. Res Reports Biodiv Studies. 2015; 4: 33–46.

28. Italiano F, Bonfanti P, Maugeri SR. Evidence of tectonic control on the geochemical features of the volatiles vented along the Nebrodi-Peloritani Mts (Southern Apennine Chain, Italy). Geofluids; 2019.

29. Casalbore D, Ingrassia M, Pierdomenico M, Beaubien SE, Martorelli E, Bigi S et al. Morphoacoustic characterization of a shallow-water mud volcano offshore Scoglio d'Africa (Northern Tyrrhenian Sea) responsible for a violent gas outburst in 2017. Mar Geol. 2020; 428: 106277.

30. Linares C, Vidal M, Canals M, Kersting DK, Amblas D, Aspillaga, et al. Persistent natural acidification drives major distribution shifts in marine benthic ecosystems. Proc Royal Soc B. 2015; 282 (1818): 20150587. https://doi.org/10.1098/rspb.2015.0587 PMID: 26511045

31. Dando PR, Aliani S, Arab H, Bianchi CN, Brehmer M, Cocito S et al. Hydrothermal studies in the Aegean Sea. Physics and Chemistry of the Earth, Part B: Hydrology, Oceans and Atmosphere. 2000; 25(1): 1–8.

32. González FJ, Rincón-Tomás B, Somoza L, Santofimia E, Medialdea T, Madureira et al. Low-temperature, shallow-water hydrothermal vent mineralization following the recent submarine eruption of Tagoro volcano. Mar Geol 2020; 430: 106333.

33. Melián G, Somoza L, Padrón E, Pérez M, Hernández PA, Sumino et al. Surface CO2 emission and rising bubble plumes from degassing of crater lakes in São Miguel Island, Azores. Geol Soc Spec Publ London; 2017; 437 (1): 233–252.

34. Pérez NM, Hernández PA, Padilla G, Nolasco D, Barrancos J, Melían G et al. Global CO2 emission from volcanic lakes. Geology. 2011; 39: 235–238.

35. Peccerillo A, De Astis G, Faraone D, Forni F, Frezzotti M L. Compositional variations of magmas in the Aeolian Arc: implications for petrogenesis and geodynamics. Geol Soc Mem, London; 2013; 37: 491–510.

36. Crisa A, Lanza S, Randazzo G. The Historical Evolution of the Tindari-Marinello Spit (Patti, Messina, Italy). In Sand and Gravel Spits. Springer, Cham. 2015 pp. 103–121.

37. Cultrera F, Barreca G, Ferranti L, Monaco C, Pepe F, Passaro S, et al. Structural architecture and active deformation pattern in the northern sector of the Aeolian-Tindari-Letojanni fault system (SE Tyrrhenian Sea-NE Sicily) from integrated analysis of field, marine geophysical, seismological and geodetic data. Ital J Geosci. 2017; 136: 3.

38. Cultrera F. et al. Active faulting and continental slope instability in the Gulf of Patti (Tyrrhenian side of NE Sicily, Italy): a field, marine and seismological joint analysis. Nat Haz. 2017; 86: 5253.

39. Barberi F, Gasparini P, Innocenti F. Villari L. Volcanism of the southern Tyrrhenian Sea and its geodynamics implications. J Geophys Res. 1973; 78(23): 5221–5232.

40. Dewey JF, Helman ML, Turco E, Knott SD. Hutton DHW. Kinematics of the Western Mediterranean. Ed. Alpine tectonics, Coward M.P 1989: Geol Soc Spec Publ. 45: 265–283.

41. Faccenna C, Becker TW, Lucente FP, Jolivet L, Rossetti F. History of subduction and back-arc extension in the central Mediterranean. Geophys J Int. 2001; 145: 809–820.

42. Romano D. Gattuso A, Longo M, Caruso C, Lazzaro G, Corbo A. et al. Hazard scenarios related to submarine volcanic-hydrothermal activity and advanced monitoring strategies: A study case from the Panarea volcanic group (Aeolian islands, Italy). Special Issue Emerging Techniques for Monitoring Geofluids and Geothermal Activities. Geofluids. 2019: 1–15.

43. Esposito A, Giordano G, Anzidei M. The 2002–2003 submarine gas eruption at Panarea volcano (Aeolian Islands, Italy): Volcanology of the seafloor and implications for the hazard scenario. Mar Geol. 2006; 227(1–2): 119–134.

44. Dickson AG, Sabine CL, Christian JR. Guide to Best Practices for Ocean CO_2 Measurements, Vol. 3. Sidney. Canada: PICES Special Publication, 2007.

45. Urbini L, Ingrosso G, Djakovac T, Piacentino S, Giani M. Temporal and spatial variability of the CO_2 system in a riverine influenced area of the Mediterranean Sea, the northern Adriatic. Front Mar Sci. 2020; 7: 679.

46. Hansen HP and Koroleff F. Determination of nutrients. Grasshoff K, Kremling K, Ehrhardt M (Eds). Methods of Seawater Analysis. Weinheim: Wiley-VCH; 1999. pp 159–228.

47. Fonselius SH. Determination of hydrogen sulphide. Grasshof K, Ehrhardt M, Kremling K (Eds). Methods of Seawater Analysis. Verlag Chemie, Weinheim 1983. pp 73–80.

48. Italiano F, Sasmaz A, Yuce G. Okan OO. Thermal fluids along the East Anatolian Fault Zone (EAFZ): Geochemical features and relationships with the tectonic setting. Chem Geol. 2013; 339: 103–114.

49. Irigoyen AJ, Galván DE, Venerus LA, & Parma AM (2013). Variability in abundance of temperate reef fishes estimated by visual census. PLoS One (2013); 8(4): e61072. https://doi.org/10.1371/journal.pone.0061072 PMID: 23593395

50. Anderson MJ, Gorley RN, Clarke KR. PERMANOVA+for PRIMER: Guide to Software and Statistical Methods. PRIMER-E, Plymouth, UK. 2008. 214 pp.

51. Clarke KR, Warwick RM. Change in marine communities: an approach to statistical analysis and interpretation. 2nd edition. PRIMER-E, Plymouth, UK, 2001. 859 pp.

52. Kroeker K, Micheli F, Gambi MC & Martz T.R. Divergent ecosystem responses within a benthic marine community to ocean acidification. Proc Natl Acad Sci. 2011; 108 (35): 14515–14520. https://doi.org/10.1073/pnas.1107789108 PMID: 21844331

53. Fabricius KE, Kluibenschedl A, Harrington L, Noonan S, De'ath G. In situ changes of tropical crustose coralline algae along carbon dioxide gradients. Sci Rep. 2015; 5(1): 1–7. https://doi.org/10.1038/srep09537 PMID: 25835382

54. Caldeira K, Wickett ME. Ocean model predictions of chemistry changes from carbon dioxide emissions to the atmosphere and ocean. J Geophys Res Oceans. 2005; 110: C9.

55. Figuerola B, Hancock AM, Bax N, Cummings VJ, Downey R, Griffiths HJ et al. A review and meta-analysis of potential impacts of ocean acidification on marine calcifiers from the Southern Ocean Front Mar Sci. 2021; 8: 24.

56. Hofmann GE, Smith JE, Johnson KS, Send U, Levin LA, Micheli F et al. High-Frequency Dynamics of Ocean pH: A Multi-Ecosystem Comparison. PLoS One. 2011; 6: 12.

57. Boatta F, D'Alessandro W, Gagliano AL, Liotta M, Milazzo M, Rodolfo-Metalpa R et al. Geochemical survey of Levante Bay, Vulcano Island (Italy), a natural laboratory for the study of ocean acidification. Mar Poll Bull. 2013; 73(2): 485–494.

58. Esposito V, Auriemma R, De Vittor C, Relitti F, Urbini L, Kralj M et al. Structural and functional analyses of motile fauna associated to *Cystoseira brachycarpa* along a gradient of ocean acidification in a CO2 vent system off Panarea island (Aerolian Islands, Italy). J Mar Sci Eng. 2022; 10: 451.

59. Gugliandolo C, Italiano F, Maugeri T. The submarine hydrothermal system of Panarea (Southern Italy): biogeochemical processes at the thermal fluids-sea bottom interface. Ann Geophys 2006; 49: 2–3.

60. Mirasole A, Signa G, Gianguzza P, Bonaviri C, Mazzola A, Vizzini et al. Fish assemblages cope with ocean acidification in a shallow volcanic CO2 vent benefiting from an adjacent recovery area. Mar Environ Res. 2020; 157:104851. https://doi.org/10.1016/j.marenvres.2019.104851 PMID: 32275499

61. Foo SA, Byrne M. Forecasting impacts of ocean acidification on marine communities: Utilizing volcanic CO$_2$ vents as natural laboratories. Glob. Change Biol. 2021; 27(10): 1995–1997.

62. Zitoun R, Connell SD, Cornwall CE, Currie KI, Fabricius K, Hoffmann LJ, et al. A unique temperate rocky coastal hydrothermal vent system (Whakaari–White Island, Bay of Plenty, New Zealand): constraints for ocean acidification studies. Mar Freshw Res. 2019; 71(3): 321–344.

63. Sano Y, Wakita H, Italiano F, Nuccio MP. Helium isotopes and tectonics in southern Italy. Geophys Res Lett. 1989; 16(6): 511–514.

64. Goodwin C, Rodolfo-Metalpa R, Picton B. Hall-Spencer JM. Effects of ocean acidification on sponge communities. Mar Ecol. 2013; 35: 41–49.

65. Mirasole A, Badalamenti F, Di Franco A, Gambi MC, Teixidó N. Boosted fish abundance associated with Posidonia oceanica meadows in temperate shallow CO$_2$ vents. Sci Total Envir. 2021; 771: 145438.

66. Franke A, Clemmesen C. Effect of ocean acidification on early life stages of Atlantic herring (*Clupea harengus* L.). Biogeosciences, 2011; 8(12): 3697–3707.

67. Commission European. Guidelines for the establishment of the Natura 2000 network in the marine environment. Application of the Habitats and Birds Directives; 2007.